CHAPTER

# Agile transmission techniques

6

**Srikanth Pagadarai[1], Rakesh Rajbanshi[2], Gary J. Minden[3], and Alexander M. Wyglinski[1]**

[1]Worcester Polytechnic Institute, United States
[2]Cisco Systems, United States
[3]The University of Kansas, United States

## 6.1 INTRODUCTION

In Chapter 3, the physical (PHY) layer fundamentals concerning the use of orthogonal frequency division multiplexing (OFDM) are described. Several underlying principles and the resulting advantages confirm the efficiency with which OFDM enables high-speed wireless communications. However, an important assumption in Chapter 3 is that the radio frequency (RF) spectrum utilized by the transceiver system is based on the traditional command-and-control allocation policy followed by most regulatory bodies like the Federal Communications Commission (FCC). That is, contiguous spectrum is available for use. However, recent spectrum measurement studies have shown that the utilization of spectral resources over time, frequency, and space in such a scenario is quite low. For example, Figure 6.1 shows a snapshot of the power spectral density (PSD) from 88 MHz to 2686 MHz measured on July 11, 2008, in Worcester, Massachusetts. This figure clearly shows the presence of several unused portions of the spectrum. The presence of unused but licensed bands creates an artificial scarcity of available spectrum. Several methodologies have been proposed to efficiently utilize these noncontiguous portions of spectrum to improve spectral efficiency. This chapter focuses primarily on one family of these spectral efficiency techniques; however, the PHY layer design issues that need to be taken into consideration when those techniques are employed in the transceiver are explored in the following sections.

The choice of a physical layer transmission technique is a very important design decision when implementing a cognitive radio. In particular, the technique must be sufficiently agile to enable unlicensed users to transmit in a licensed band while not interfering with the incumbent users. Moreover, to support throughput-intensive


Doi: 10.1016/B978-0-12-374715-0.00006-X

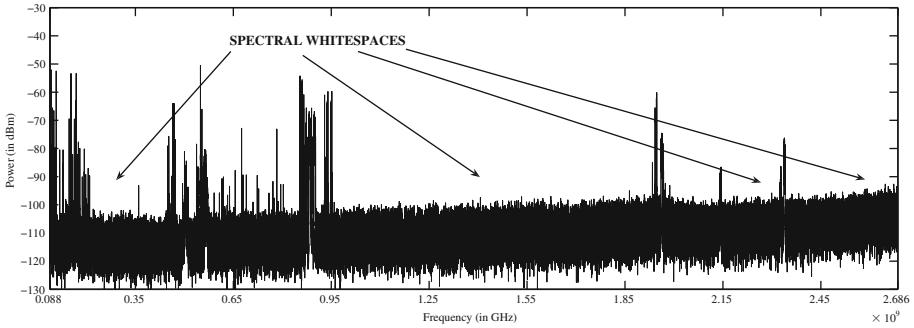


**FIGURE 6.1**

A snapshot of PSD from 88 MHz to 2686 MHz measured on July 11, 2008, in Worcester, Massachusetts ($N42^o16.36602,\ W71^o48.46548$).

applications, the technique should be capable of handling high data rates. One technique that meets both these requirements is a variant of orthogonal frequency division multiplexing called *noncontiguous OFDM* (NC-OFDM) [181]. Compared to other techniques, NC-OFDM is capable of deactivating subcarriers across its transmission bandwidth that could potentially interfere with the transmission of other users. Moreover, NC-OFDM can support a high aggregate data rate with the remaining subcarriers and simultaneously maintain an acceptable level of error robustness. Despite the advantages of NC-OFDM, two critical design issues are associated with this technique. First, the detection of the white spaces in the licensed bands for secondary-user transmissions. Radio parameter adaptation and hardware reconfiguration are another crucial requirement.

As mentioned earlier in this chapter, we discuss the techniques that need to be employed in a dynamic, spectrally agile, hardware-reconfigurable software-defined radio (SDR) to alleviate some of the problems arising due to secondary transmissions in an already licensed band. This chapter is organized as follows. Section 6.2 presents a classification of the spectrum sharing techniques in the existing literature. Next, in Section 6.3, we describe the transceiver system that employs these spectrum sharing techniques. In Section 6.4, we discuss some of the issues resulting from the use of noncontiguous bands, such as interference to the primary users, the need for fast Fourier transform (FFT) pruning, and the need for peak-to-average power ratio (PAPR) reduction. We then conclude the chapter with several remarks and comments in Section 6.5.

## 6.2 WIRELESS TRANSMISSION FOR DYNAMIC SPECTRUM ACCESS

Figure 6.2 shows a dynamic spectral access (DSA) scenario that is viewed as a solution to the problem of the artificial spectral scarcity. As shown in this figure, at any time instant, several noncontiguous spectral regions are left unused. These

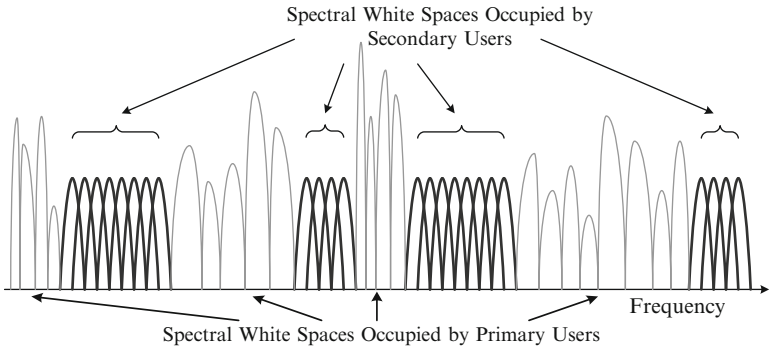


**FIGURE 6.2**

The utilization of noncontiguous regions of spectrum for wireless transmission.

unused portions can be used by secondary users for high-speed wireless communications while simultaneously ensuring that the primary user's rights are not violated. This idea of using multiple noncontiguous portions of spectrum is referred to as *spectrum pooling*.

### 6.2.1 Spectrum Pooling

The notion of "spectrum pooling," first introduced in [6], is a mechanism for pooling the spectral resources from different spectral owners and renting these spectral resources to unlicensed users during idle periods. However, such a lease of licensed spectral resources to rental users, while providing additional revenue to the licensed users, brings forth many technological, juristical, economic, and political questions concerning the regulatory aspects of spectrum pooling. The technical challenges that need to be solved to make spectrum pooling practical have been the research focus of numerous groups at universities all over the world.

Flexible pooling of the spectral resources is an important requirement for future cognitive radios to enable efficient secondary utilization of the spectrum [182]. Such a cognitive radio needs to employ agile physical layer transmission techniques to respect the rights of the incumbent licensed users and reconfigurable hardware that makes the adaptation to changing environmental conditions feasible [183]. Moreover, a formal radio etiquette needs to be formulated, which is a framework to moderate the use of the RF spectrum for guaranteeing the rights of the licensed users as well as for the flexible coordination between the unlicensed users.

### 6.2.2 Underlay and Overlay Transmission

Spectrum sharing techniques can be classified into *underlay* and *overlay* spectrum sharing based on the spectrum access techniques. Underlay systems use ultra-wideband (UWB) [184, 185] or spread-spectrum techniques, such as code division multiple access (CDMA) [186], to transmit the signal below the noise floor of the

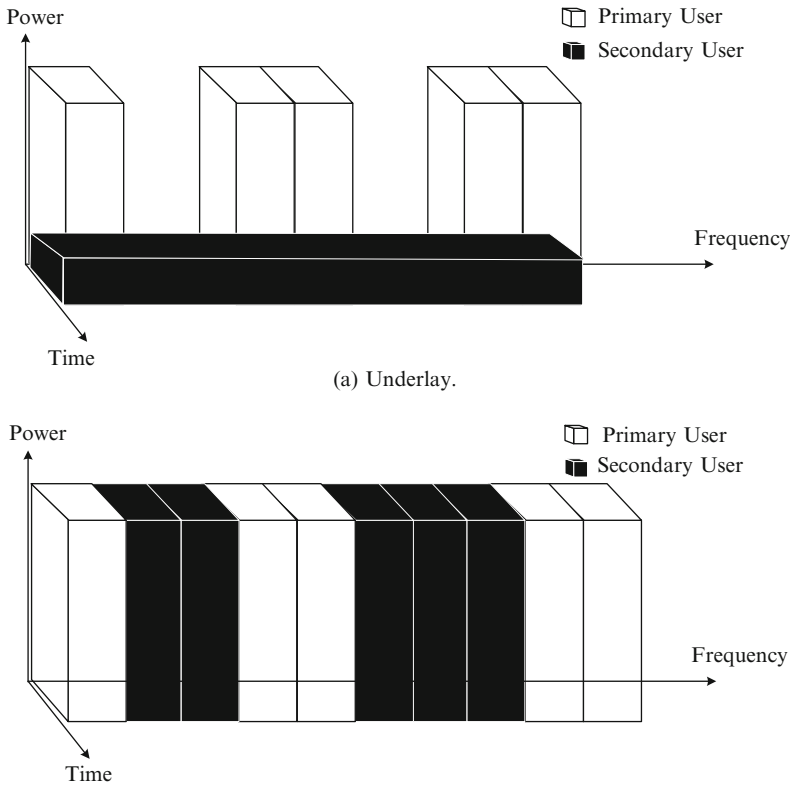


**FIGURE 6.3**

Overlay and underlay spectrum sharing.

spectrum [187]. An example of the time- and frequency-domain information of an underlay spectrum sharing system is shown in Figure 6.3(a). In this figure, we see that the underlay systems use wideband low-power signals for transmissions. However, this technique can increase the overall noise temperature and thereby worsen error robustness of the primary users as compared to the case without underlay systems. To avoid any interference to the primary users, the underlay system can use interference avoidance techniques, such as *notching* [188] and *waveform adaptation* [189].

The spectrum holes[1] filled in by secondary transmissions in an overlay system are shown in Figure 6.3(b). When interference among the users is high, it has been shown that frequency division multiplexing is an optimal technique [190].

[1] A *spectrum hole* is an unused portion of the licensed spectrum [11].

As shown in this figure, the overlay systems use the unoccupied portions of the spectrum with guard intervals for secondary transmissions, keeping the interference to the primary users to a minimum. Since the licensed system has privileged access to the spectrum, it must not be disturbed by any secondary transmissions. This results in two main design goals for an overlay system [191]:

- Minimum interference to licensed transmissions.
- Maximum exploitation of the gaps in the time–frequency domain.

To achieve these goals, the overlay system needs information about the spectrum allocation of the licensed systems, for example, by regularly performing spectrum measurements. As explained previously, spectral pooling represents the idea of storing this information by merging spectral ranges from different spectrum owners (military, trunked radio, etc.) into a common pool, where users may temporarily rent spectral resources during idle periods of licensed users, thereby enabling the secondary utilization of already licensed frequency bands [24]. In a spectrum pooling system, a centralized entity can collect measurement information gathered by the secondary-user terminals during the detection cycle and maintain the spectrum usage information. The centralized entity is responsible for making decisions on granting portions of the spectrum to the secondary users. With the use of a centralized entity, the information management of a spectrum access network would be relatively simple. However, this same entity can also easily be a bottleneck for the network due to the associated information exchange overhead. Since the overlay systems can readily exploit the unused portions of the spectrum without interfering with the incumbent users and without increasing the noise temperature of the system, we consider only overlay systems in this chapter from this point forward.

One of the most challenging problems of spectrum sharing systems is their successful coexistence in the same frequency band; that is, an overlay system should not degrade the performance of systems already working in the target frequency band. For instance, out-of-band radiation has to be reduced to enable coexistence. The transmitter spectral mask is a measure of the transmitter spectral profile to verify that the device is not transmitting excessive amounts of energy outside its assigned channel bandwidth. Several approaches have been proposed in literature for suppressing the side lobe levels, such as the deactivation of subcarriers lying at the borders of an OFDM spectrum [192], windowing [193], subcarrier weighting [194], and insertion of cancellation carriers [195].

Despite being a solution to the problem of the apparent spectrum scarcity, dynamic spectrum access puts additional design constraints on the wireless transceiver. This is because, as multiple pockets of wireless spectrum are being utilized, the noise characteristics differ substantially across the noncontiguous bands of spectrum. Hence, a spectrally agile but extremely robust modulation technique is required for use in wireless transceivers employed in a DSA scenario. As mentioned earlier, the noncontiguous OFDM proposed in [181] satisfies these

requirements. While conventional multicarrier (MC) CDMA has proven to be effective compared to conventional OFDM systems because of its superior multiuser interference limiting capabilities, NC-OFDM has been shown to be better than noncontiguous MC-CDMA (NC-MC-CDMA) [196]. This is because the deactivation of subcarriers corresponding to primary-user transmissions causes a loss of orthogonality in NC-MC-CDMA, leading to a worse bit error rate (BER) performance than NC-OFDM systems. Therefore, in the following discussion, our focus for spectrally agile modulation techniques is NC-OFDM.

## 6.3 NONCONTIGUOUS ORTHOGONAL FREQUENCY DIVISION MULTIPLEXING

A general schematic of an NC-OFDM transceiver is shown in Figure 6.4. Without loss of generality, a high-speed data stream, $x(n)$, is modulated using $M$-ary phase shift keying (MPSK).[2] Then, the modulated data stream is split into $N$ slower data streams using a serial-to-parallel (S/P) converter. Note that the subcarriers in the NC-OFDM transceiver do not need to be all active as in conventional OFDM. Moreover, active subcarriers are located in the unoccupied spectrum bands, which are determined by dynamic spectrum sensing techniques [197]. The inverse fast Fourier transform (IFFT) is then applied to these modulated subcarrier signals. Prior to transmission, a guard interval with a length greater than the channel delay spread is added to each NC-OFDM symbol using the cyclic prefix (CP) block to mitigate the effects of intersymbol interference (ISI). Following the parallel-to-serial (P/S) conversion, the baseband NC-OFDM signal, $s(n)$, is passed through the transmitter radio frequency chain, which amplifies the signal and up-converts it to the desired center frequency.

The receiver performs the reverse operation of the transmitter, mixing the RF signal to the baseband for processing, yielding the signal $r(n)$. Then, the signal is converted into parallel streams using the S/P converter, the CP is discarded, and the FFT is applied to transform the time domain data into the frequency domain. After compensating distortion introduced by the channel using equalization, the data in the active subcarriers are multiplexed using a P/S converter, and demodulated into a reconstructed version of the original high-speed input, $\hat{x}(n)$.

From this system overview, we observe that the spectrum sensing, spectrum shaping, peak-to-average power ratio, radio parameter adaption, and efficient radio implementation are critical issues associated with an OFDM-based cognitive radio. In the next section, we will describe these issues and ways to mitigate them in order to develop efficient OFDM-based cognitive radios.

[2]Other forms of digital modulation, including $M$-ary quadrature amplitude modulation, can also be employed by the transceiver.

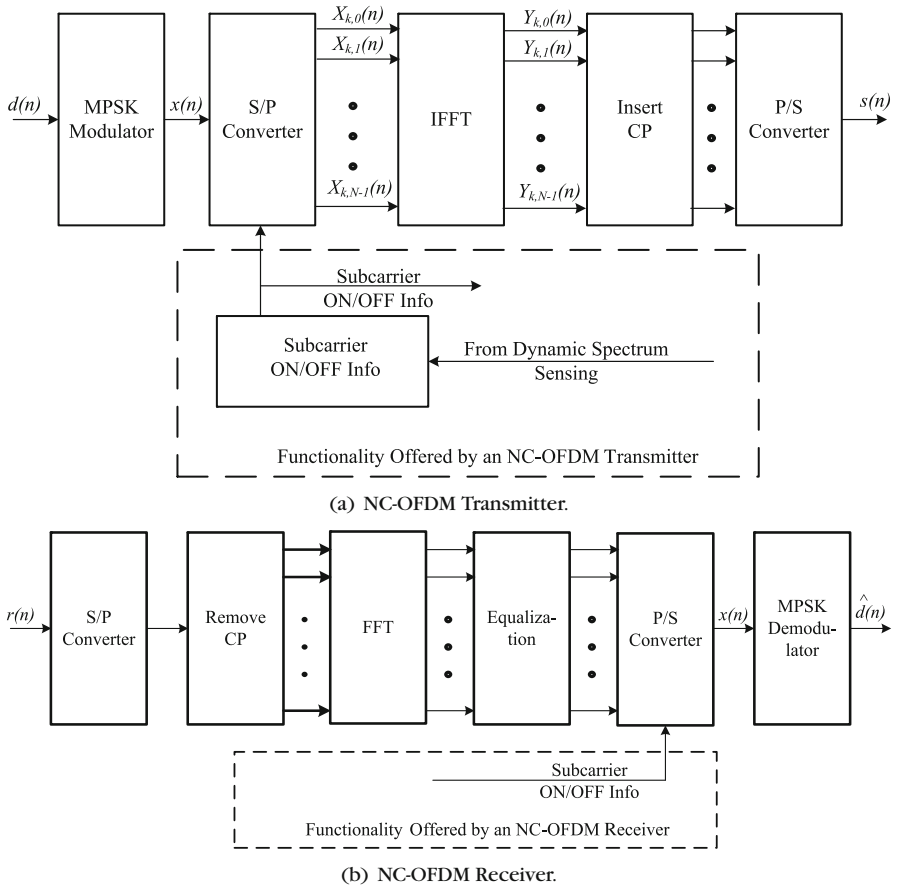


**FIGURE 6.4**

An NC-OFDM transceiver.

## 6.4 NC-OFDM-BASED COGNITIVE RADIO: CHALLENGES AND SOLUTIONS

The digital modulation scheme based on orthogonal frequency division multiplexing is the natural approach for DSA due to inherent frequency subbanding. OFDM spectrum access is scalable while keeping users orthogonal and noninterfering provided the users are synchronized. However, the conventional OFDM scheme does not provide truly band-limited signals due to spectral leakage caused by sync-pulse-shaped transmission resulting from the IFFT operation. This may cause interference to the adjacent band primary users proportional to the power allocated to the

cognitive user on the corresponding adjacent subcarrier. Therefore, an OFDM transmitter must be adapted.

### 6.4.1 Interference Mitigation

Figure 6.5 shows the power spectral density of an OFDM-modulated carrier. This figure shows the subcarrier spacing and the interference power due to the first side lobe in the first adjacent band. It is observed that, as the distance between the location of the subcarrier of the rental system and the considered subband increases, the interference caused by it reduces monotonically, which is a characteristic of the *sinc* pulse. However, it should also be noted that, in a practical scenario consisting of $N$ subcarriers, the actual value of the interference caused in a particular legacy system subband is a function of the random symbols carried by the *sinc* pulses and $N$.

With respect to the interference caused by the unlicensed user to the licensed user, the important issue that needs to be taken into consideration when designing an OFDM-based overlay system is that its impact on the legacy system should be very small. Thus, the basic aim of any algorithm for side lobe suppression is to reduce the side lobe power levels while causing little or no effect to the other

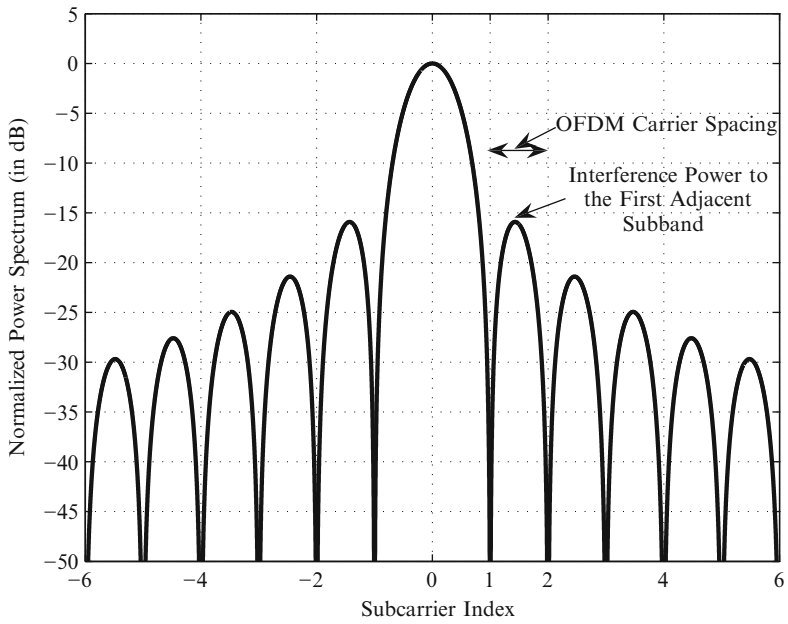


**FIGURE 6.5**

The interference due to one OFDM-modulated carrier.

secondary system parameters. Before moving on to a summary of the existing algorithms for side lobe suppression, a brief mathematical representation of the interference to the legacy system and two simple techniques for mitigating its effects are provided in this section.

Assuming the transmit signal $s(t)$ on each subcarrier of the OFDM transceiver system is a rectangular non-return-to-zero (NRZ) signal, the power spectral density of $s(t)$ is represented in the form [108]

$$\Phi_{ss}(f) = A^2 T \left( \frac{\sin \pi f T}{\pi f T} \right)^2 , \tag{6.1}$$

where $A$ denotes the signal amplitude and $T$ is the symbol duration that consists of the sum of symbol duration, $T_S$, and guard interval, $T_G$. The assumption that the transmit signal $s(t)$ on each subcarrier is a rectangular NRZ signal is valid since it matches the wireless local area network (LAN) standards [198, 199]. Now, assuming that the legacy system is located in the vicinity of the rental system, the mean relative interference, $P_{\text{Interference}}(n)$, to a legacy system subband is defined as [192]

$$P_{\text{Interference}}(n) = \frac{1}{P_{\text{Total}}} \int_n^{n+1} \Phi_{ss}(f) df, \tag{6.2}$$

where $P_{\text{Total}}$ is the total transmit power emitted on one subcarrier and $n$ represents the distance between the considered subcarrier and the legacy system in multiples of $\Delta f$.

The idea of interference calculation for the case of one subcarrier can be extended to a system with $N$ subcarriers. Let $s_n(x)$, $n = 1, 2, 3, ..., N$ be the subcarrier of index $n$ represented in the frequency domain. Then,

$$s_n(x) = a_n \frac{\sin[\pi(x - x_n)]}{\pi(x - x_n)}, \qquad n = 1, 2, ....., N. \tag{6.3}$$

In this equation, $\mathbf{a} = [a_1 \; a_2 \; \cdots \; a_N]^T$ is a data symbol array, and $x$ is a normalized frequency given by

$$x = (f - f_0)T,$$

where $f$ denotes the frequency and $f_0$ is the center frequency. Also, $x_n$ is the normalized center frequency of the $n$th subcarrier. Again, the signal in the time domain at the transmitter is assumed to be in a rectangular NRZ form. Now, the OFDM symbol in the frequency domain over the $N$ subcarriers is

$$S(x) = \sum_{n=1}^{N} s_n(x). \tag{6.4}$$

The power spectral density of this signal is given by

$$\Phi_{ss}(f) = |S(x)|^2 = \left| \sum_{n=1}^{N} a_n \frac{\sin[\pi(x - x_n)]}{\pi(x - x_n)} \right|^2 . \tag{6.5}$$

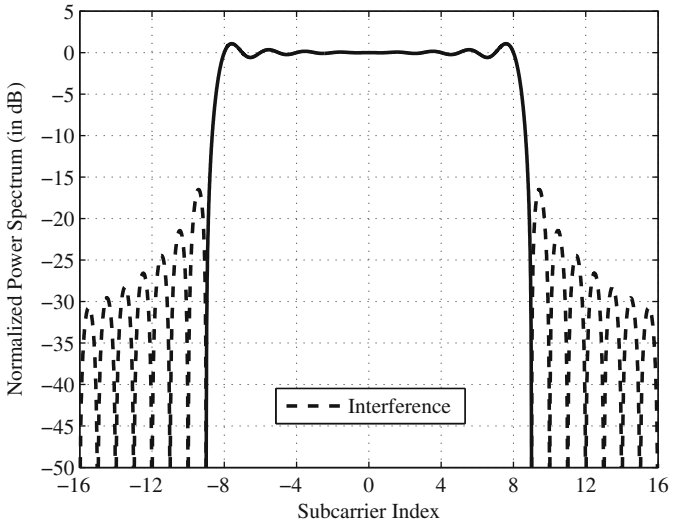


**FIGURE 6.6**

The interference in a BPSK-OFDM system with 16 subcarriers.

As an example, a BPSK-OFDM system with $N = 16$ subcarriers is considered. When the vector $\mathbf{a} = [1\ 1\ 1\ 1\ 1\ 1\ 1\ 1\ 1\ 1\ 1\ 1\ 1\ 1\ 1\ 1]^T$, Figure 6.6 shows the normalized OFDM power spectrum. As shown in this figure, the portion of the signal indicated in dashed lines represents the potential interference causing side lobes, resulting from summing up the sinc pulses that carry the symbols from the data vector. Also, Figure 6.6 is for the case where the data vector consists of ones and, hence, depending on the random distribution of the symbols, the side lobe power levels decay at different rates.

### *Windowing*

One of the simplest and the earliest solutions offered to counter the effects of OOB interference is windowing the OFDM transmit signal in the time domain [192,193]. A raised cosine window defined by

$$w(t) = \begin{cases} \frac{1}{2} + \frac{1}{2}\cos\left(\pi + \frac{\pi t}{\beta T}\right), & \text{for } 0 \le t < \beta T \\ 1, & \text{for } \beta T \le t < T \\ \frac{1}{2} + \frac{1}{2}\cos\left(\frac{\pi(t-T)}{\beta T}\right), & \text{for } T \le t < (1+\beta)T \end{cases} \tag{6.6}$$

is a commonly used window type where $\beta$ is defined as the roll-off factor. Applying the transmit filter, $w(t)$, the OFDM signal in time domain is as shown in Figure 6.7. It can be noted from this figure that the postfix needs to be longer than $\beta T$ to maintain the orthogonality within the OFDM signal. That is, the application of windowing to reduce the out-of-band radiation of the OFDM signal has the adverse

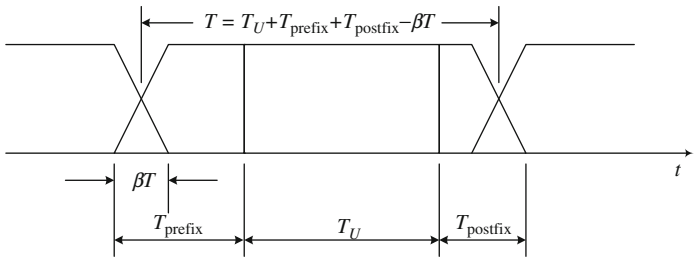


**FIGURE 6.7**

Structure of the temporal OFDM signal using a raised cosine window.

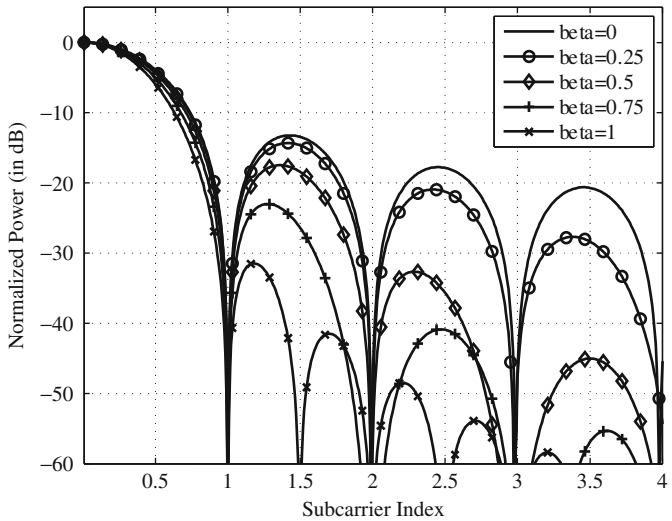


**FIGURE 6.8**

Impact of roll-off factor on the PSD of the rental system signal.

effect of expanding the temporal symbol duration by $(1+\beta)$, resulting in a lowered system throughput for the unlicensed user.

The impact of the roll-off factor of the raised cosine window on the side lobe power levels of the OFDM symbol is depicted in Figure 6.8. It can be observed from this figure that, for smaller values of $\beta$, the suppression achieved in the side lobe power levels of the first adjacent band is very small. As the distance between the location of the subcarrier of the rental system and the considered subband increases, the suppression achieved also increases. Also, for very large values of $\beta$, the suppression achieved is considerable even in the case of the first adjacent band. However, the symbol duration in time is also increased, which reduces the

system throughput. Therefore, windowing can be applied as an additional means to suppress the high side lobes, but more powerful techniques need to be developed.

### Insertion of Guard Bands

Another technique for mitigating the effects of the side lobes from the secondary user's OFDM symbols on the system performance of the legacy system is to deactivate additional subcarriers in the vicinity of the licensed user that are allotted to the unlicensed user in addition to those that are deactivated due to licensed user accesses [193]. With this technique, the already scarce spectral resources are wasted. Moreover, the reduction achieved is not significant enough, as shown in Figure 6.9.

In this figure, a BPSK-OFDM system with $N = 64$ subcarriers is considered. The simulations were performed over 20,000 symbols. From Figure 6.9(a), it can be observed that, by inserting two guard carriers (GCs) on each side of the spectrum, the achievable average reduction of the maximum interference causing side lobe is only 2.8 dB, and by inserting eight guard carriers, the reduction achieved is around 4.6 dB. A significant reduction of around 10 dB can be achieved, by giving up 25% of the allocated bandwidth; that is, by using 16 subcarriers out of 64 for inserting guard bands. The complementary cumulative distribution function (CCDF) of Figure 6.9(b) also illustrates the same point. On average, 99.9% of the side lobe power is below $-3.8$ dB in the original case, whereas by inserting two guard carriers on each side of the OFDM spectrum, the value is $-8.7$ dB, and by inserting eight guard carriers, the value is around $-15$ dB.

### Existing Solutions

Insertion of cancellation carriers is one of the most common approaches to achieve side lobe suppression. The working principle behind this technique is described in the following paragraphs.

Suppose we define the total number of subcarriers that can be transmitted by a secondary user in a spectral white space as $L = L_A + L_{CC}$, where $L_A$ is the number of active subcarriers used for signal transmission, and $L_{CC}$ is the total number of subcarriers reserved for inserting cancellation subcarriers. As a result, the equations describing the individual subcarriers and the cumulative OFDM signal can be expressed as

$$s_{l_a}(y) = d_{l_a} \frac{\sin\left[\pi\left(y - y_{l_a}\right)\right]}{\pi\left(y - y_{l_a}\right)}, \quad l_a = -L_A/2, ...., L_A/2, \tag{6.7}$$

and

$$S(y) = \sum_{l_a=-L_A/2}^{L_A/2} s_{l_a}(y). \tag{6.8}$$

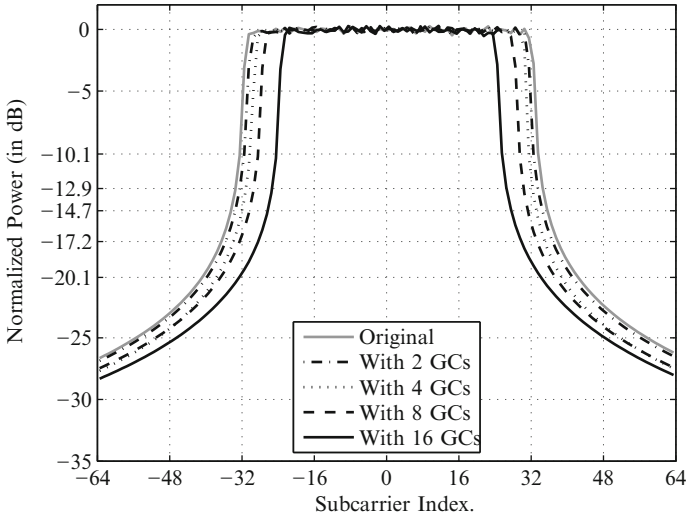


(a) Normalized power spectrum plot.

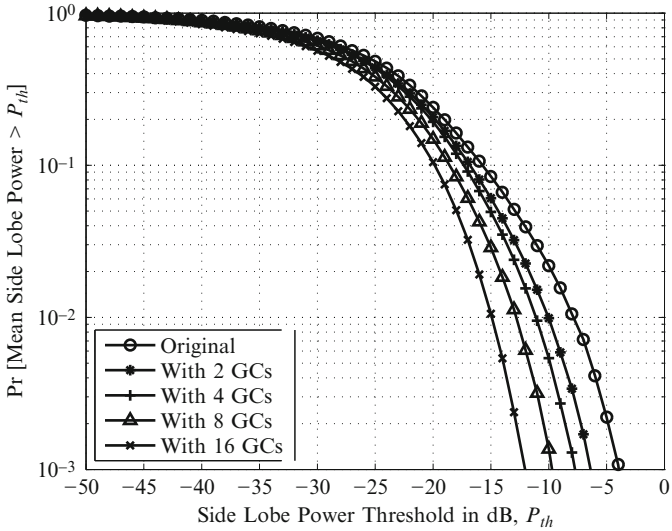


(b) Complementary cumulative distribution function plot.

**FIGURE 6.9**

Interference suppression in a BPSK-OFDM system with 64 subcarriers by inserting guard subcarriers.

Since the frequency response of an OFDM subcarrier is represented by the *sinc* function, the side lobe power levels of the composite signal, at any frequency location that consists of superposed and frequency-translated subcarriers, can be algebraically computed as the sum of the side lobe powers of each *sinc* function at that location given the input sequence. Therefore, if $I_k$ represents the side lobe amplitude level at the $k$th frequency index (in the out-of-band, OOB, region) normalized to the subcarrier bandwidth, then we can express this amplitude level as

$$I_k = \sum_{l_a=-L_A/2}^{L_A/2} s_{l_a}(k). \tag{6.9}$$

Suppose the amplitude level of the cancellation subcarrier inserted at $j = L_A/2 + 1$ to nullify the side lobe at the $k = L/2 + 1$ frequency index is selected in such a way that it possesses a side lobe at the $k$th frequency index, which is equal in amplitude but opposite in sign to $I_k$. In other words, we select $C_j$ such that it reduces the interference $I_k$. A simple solution is to select $C_j$ such that $C_k = -I_k$. Figure 6.10 illustrates this procedure for a 16-subcarrier BPSK system, where $L_A = 14$ and $L_{CC} = 2$. Suppose the symbol sequence transmitted over the active subcarriers is [1 1 1 1 1 1 1 1 1 1 1 1 1 1]. The superscripts $r$ and $l$ are used to signify, respectively, the side lobe power levels on the right and left sides of the OFDM signal spectrum. While choosing the symbol values over subsequent cancellation subcarriers (CCs) in a scenario where multiple cancellation subcarriers

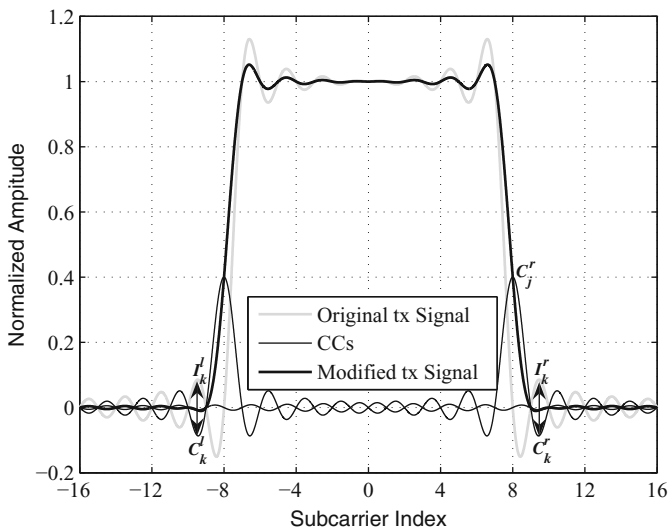


**FIGURE 6.10**

Side lobe power reduction with cancellation carriers.

are inserted on each side of the signal spectrum, the side lobe regrowth over the locations nulled by the previously inserted CCs is constrained to be minimal.

In the case of multiple cancellation subcarriers, the symbols over cancellation subcarriers are computed iteratively for minimizing the side lobe power. The symbol over the first cancellation subcarrier is computed such that it nullifies the first OOB side lobe amplitude. The symbol over the second cancellation subcarrier is computed for minimizing the second OOB side lobe amplitude. The procedure can be continued for a given number of cancellation subcarriers until the desired side lobe power levels are achieved. If the desired suppression is higher, a greater portion of the bandwidth has to be allocated to insert additional cancellation subcarriers. However, significant side lobe power suppression can be achieved with a small number of CCs, resulting in a reasonable trade-off between bandwidth reduction and achievable interference suppression. This technique described is illustrated in the form of a flow diagram in Figure 6.11.

Another approach proposed in [201] is the constellation expansion (CE) technique, wherein the symbols obtained by modulating the input bit sequence to a $2^k$ constellation space are mapped to an expanded constellation space consisting of $2^{k+1}$ constellation points. In other words, for every constellation point in the original symbol sequence, there are two points to choose from in the expanded constellation space. Selecting one of the points on a random basis, each symbol in a sequence of $N$ symbols is mapped to $N$ symbols from the expanded symbol set. An underlying assumption with the proposed CE technique is that the transmitter and the receiver have prior knowledge of the points of the expanded constellation that are associated with the points in the original constellation. Hence, after the demodulation process, the symbols can be remapped to the points of the original constellation. With this knowledge, no side information needed to be shared between the transmitter and the receiver. As an example, an approach for mapping QPSK symbols to an expanded constellation space is shown in Figure 6.12. The rationale behind this association of points is to take advantage of the randomness involved in selecting one of the two points, and hence the combination of different in-phase and quadrature-phase components from all the subcarriers results in a sequence with fewer side lobes.

Several other techniques for side lobe suppression based on complex optimization procedures have been proposed, such as (1) singular value decomposition optimization approaches for either inserting cancellation subcarriers [195] or weighting the subcarriers [194] to reduce the side lobe power levels over the neighboring RF spectrum, (2) reserved tones–based convex optimization technique [202] for suppressing side lobe power levels as well as the peak-to-average power ratio, and (3) a two-stage constellation expansion combined with a suboptimal cancellation carrier technique [200].

In (1), the weights are computed by selecting an optimization region, which is the portion of the neighboring RF spectrum over which the side lobes need to be suppressed and finding an optimal solution. The optimization is formulated as a linear least squares problem, solved using a singular value decomposition approach.

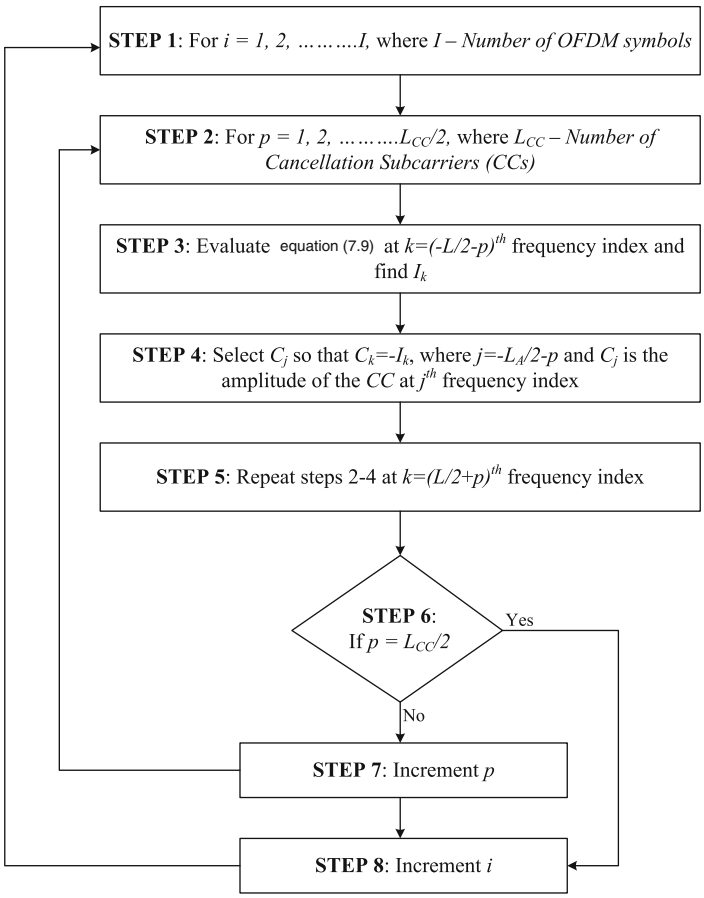


**FIGURE 6.11**

The algorithm used for inserting CCs [200].

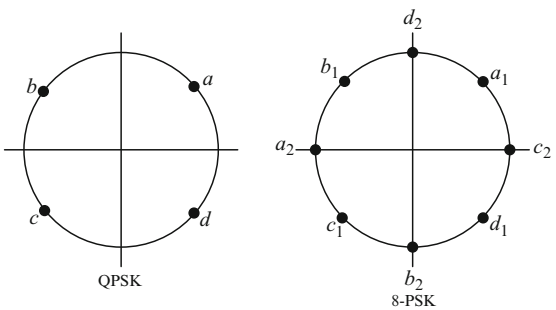


**FIGURE 6.12**

A mapping of symbols from QPSK constellation to an expanded constellation space.

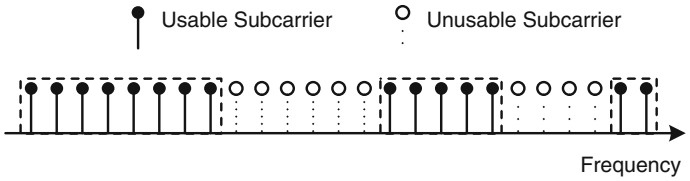


**FIGURE 6.13**

Subcarrier distribution over wideband spectrum.

In (2), a technique based on *reserved tones* is employed and the optimization problems for reducing PAPR and side lobe power levels are combined. A vector-valued objective function is obtained, and by employing a convex optimization algorithm, the optimal solution is achieved. Finally, in (3), symbols from a higher constellation are associated with symbols of the original constellation and the randomness in choosing points is exploited to achieve a symbols sequence with low side lobes. The results are combined with a suboptimal cancellation carrier approach to yield further reduction in the side lobe power levels. A summary of approaches that manipulate the data symbols to achieve a low side lobe power level is given in [203].

## 6.4.2 FFT Pruning for NC-OFDM

In a wideband communications system, a large portion of frequency channels may be occupied by transmissions from incumbent or unlicensed users. Systems that desire to operate within these occupied channels must avoid placing subcarriers in occupied or licensed spectrum. Therefore, to avoid interfering with these other transmissions, the subcarrier within the vicinity of the given transmission is turned off or nulled (Figure 6.13). In the case of systems like OFDM, these null subcarriers are represented as zero-valued inputs to the FFT and IFFT blocks. When available spectrum is sparse, the number of zero-valued inputs in the FFT may be significant relative to the total number of usable subcarriers. When the relative number of zero-valued inputs is quite large, significant hardware resources can be saved by pruning the FFT algorithm.

Channel conditions and incumbent spectrum occupancy (ISO) often vary over time, so efficient FFT pruning algorithms should be able to generate an optimized FFT implementation every time the channel conditions and ISO change. Given that the hardware resources of small form-factor cognitive radios are limited, this FFT pruning algorithm is very beneficial.

### *Fundamentals of FFT Pruning*

In Figure 6.14 an eight-point decimation in frequency (DIF) FFT butterfly structure is shown, where $a_i$ represents the $i$th input signal to the FFT block. Suppose the

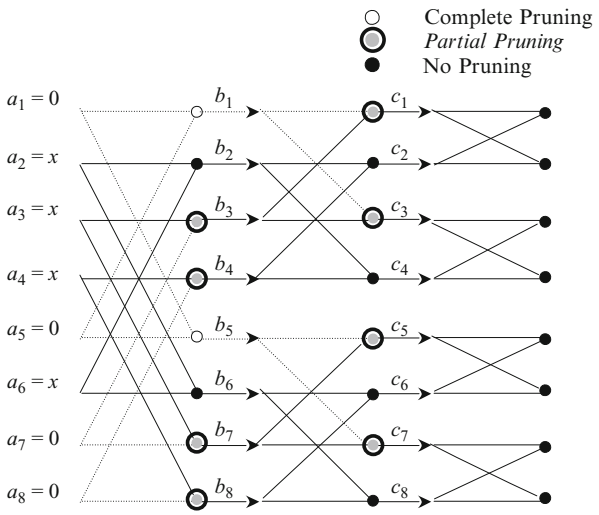


**FIGURE 6.14**

FFT butterfly structure. A value of 0 denotes a zero-valued subcarrier and *x* denotes a data-bearing subcarrier. The dotted lines represent the computations that can be pruned.

incumbent users are located at subcarriers $a_1, a_5, a_7$, and $a_8$. Therefore, input data over all these carriers must always be zero. For a conventional FFT algorithm, the total number of multiplications and additions are $N \log_2 N$. However, with an FFT pruning algorithm, the unnecessary multiplications and addition operations at stages $b_1$ and $b_5$ can be pruned as their values will always be zero. Moreover, multiplications and additions at nodes $b_3, b_4, b_7$, and $b_8$ can be replaced with a simple "copy" operation, whereas addition operations in nodes $c_1, c_3, c_5$, and $c_7$ can be pruned to save the FFT computation time. Therefore, the FFT computation time can be significantly improved with partial and complete pruning.

In wideband communication systems, the channel conditions and ISO vary over time. Therefore, the FFT pruning algorithm should be able to design an efficient FFT implementation every time the channel condition and ISO change.

### *Existing Solutions*

Alves, Osorio, and Swamy proposed an FFT pruning algorithm that operates on any zero-valued input distribution [204]. Suppose we have a radix-2 FFT algorithm with $N$ levels ($2^N$ FFT points). A matrix $M_i$, with $N$ columns and $2^N$ rows, is generated. Each element of the matrix corresponds to an addition/multiplication node of the FFT flow graph. The node needs to be computed if the corresponding element in the matrix $M_i$ is nonzero. On the other hand, if the element of the matrix is zero, the corresponding node need not be computed. To obtain the matrix $M_i$, we need a subcarrier input vector with $2^N$ elements, where each element of this

vector corresponds to each input element. If the input element is nonzero, the corresponding vector element will be unity, and if the input element is zero, the corresponding vector element will be zero. By using this input vector, we can compute the first column of the matrix $M_i$. In turn, by using the first column of the matrix $M_i$, the second column of matrix $M_i$ can be obtained, and so forth.

To save execution time, the algorithm proposed in [181] builds upon the previous algorithm by avoiding the use of conditional statements. This algorithm is based on the Cooley-Tukey divide-and-conquer algorithm that uses in-place computation [205]. For a radix-2 FFT, the Cooley-Tukey algorithm divides the problem size into two interleaved halves with each recursive stage. This approach requires the computations to be proportional to $N \log_2 N$, whereas the equivalent discrete Fourier transform (DFT) would require the computations proportional to $N^2$. In [181], the proposed algorithm operates in a similar manner. Additionally, this algorithm prunes the unnecessary multiplication and addition operations at the nodes in the FFT flow graph to reduce the execution time for the FFT computations.

### 6.4.3 Peak-to-Average Power Ratio Problem in NC-OFDM

One critical issue of an OFDM-based implementation is the potential for high PAPR. If unchecked, high PAPR could lead to *amplitude clipping*,[3] resulting in a substantial amount of distortion being introduced to the transmitted signal. Furthermore, as the number of subcarriers increases, so does the PAPR values. Therefore, several researchers developed digital baseband PAPR reduction techniques [206–212] in an attempt to solve this problem.

Due to the null subcarriers in the NC-OFDM signal, its PAPR characteristics are slightly different from those of conventional OFDM signals. Moreover, the PAPR reduction algorithms developed for conventional OFDM signals need to be modified for its usage in NC-OFDM systems. The PAPR reduction algorithms should also be aware of the deactivated subcarriers, thereby avoiding any interference to the primary user transmissions.

#### *Definition of Peak-to-Average Power Ratio*

The complex envelope of a baseband NC-OFDM signal, consisting of all $N$ contiguous subcarriers over a time interval $[0, T]$, is given by

$$s(t) = \frac{1}{\sqrt{N}} \sum_{k=0}^{N-1} A_k e^{j2\pi kt/T}, \tag{6.10}$$

where $A_k$ is the symbol of the $k$th subcarrier,[4] $T$ is the OFDM symbol duration, and $j = \sqrt{-1}$. The symbol over the $k$th deactivated subcarrier is $A_k = 0$.

[3]This occurs when the dynamic range of the digital-to-analog converter or the power amplifier is insufficient.

[4]For example, $A_k \in \{1, -1\}$ for BPSK signaling, and $A_k \in \{\pm 1, \pm j\}$ for QPSK signaling.

The PAPR of Equation (6.10) is defined as the ratio between the maximum instantaneous power and the average power of an OFDM signal, namely [213],

$$\text{PAPR}(s(t)) = \frac{\max\limits_{0\le t\le T} |s(t)|^2}{E\left\{|s(t)|^2\right\}}, \tag{6.11}$$

where $E\{.\}$ denotes the expectation operator. Without loss of generality, we can safely neglect the cyclic extension from the analysis, since it does not contribute to the PAPR problem. The continuous time PAPR of $s(t)$ can be approximated using the discrete time PAPR, which is obtained using samples of the OFDM signal, $s(n)$. It has been shown that an oversampling factor of 4 is sufficient to estimate the continuous PAPR of a BPSK system [214].

As an illustration, consider a 16 subcarrier BPSK-OFDM transceiver system. When all the input symbols are ones, the normalized power of the OFDM symbol in the time domain is as shown in Figure 6.15(a). From this figure, the mean power of the signal can be calculated to be 0.0625 and the peak power is unity. The PAPR of the signal is 16. Now, consider an input random sequence, [1 1 1 −1 1 1 −1 −1 1 1 −1 −1 1 −1 −1 −1]. The normalized power of the OFDM symbol in the time domain is shown in Figure 6.15(b). The mean power of the signal remains 0.0625 as the total power of the signal remains constant. However, the peak power is 0.3025. Thus, the PAPR is equal to 4.8407. This figure illustrates that the random sequence being transmitted has an effect on the PAPR of the signal. Moreover, it has been suggested that the sequences with the maximum correlation yield a very high PAPR value [215]. Some of the algorithms proposed in the literature aim at reducing the correlation of the sequence to reduce the PAPR. Furthermore, the PAPR of a system is directly related to the number of subcarriers in the system. The greater the number of subcarriers, the larger is the PAPR.

### *Existing Solutions*

Subcarrier power adjustment–based techniques are one of the most popular approaches in the technical literature for combating PAPR. Power adjustment approaches can be further classified into approaches that constrain the total power of all the subcarriers [216, 217] and those that constrain the power of subcarriers in a window [218, 219].

Total power-constrained power adjustment implies that, if power of any subcarrier is reduced or turned off, the excess power allocated to it can be transferred to the remaining active subcarriers. Let $\pi_k$ be the transmitted power of the $k$th subcarrier ($k = 0, 1, \ldots, N-1$). If the total number of subcarriers is $N$, the power constraint is given by

$$\sum_{k=0}^{N-1} \pi_k = \pi_{\text{total}}. \tag{6.12}$$

The aggregate bit rate is approximately maximized if the bit error rates in all the subbands are equal, whereas BER performance is optimized when all the

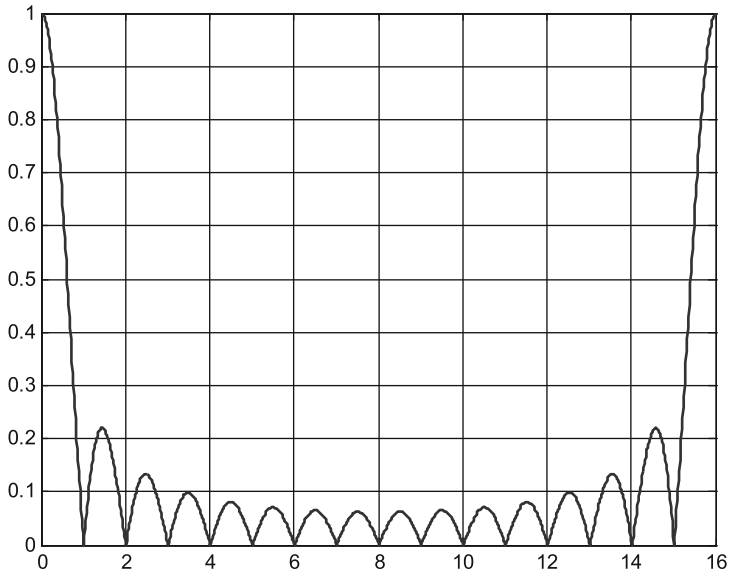


(a) An *all-ones* symbol sequence.

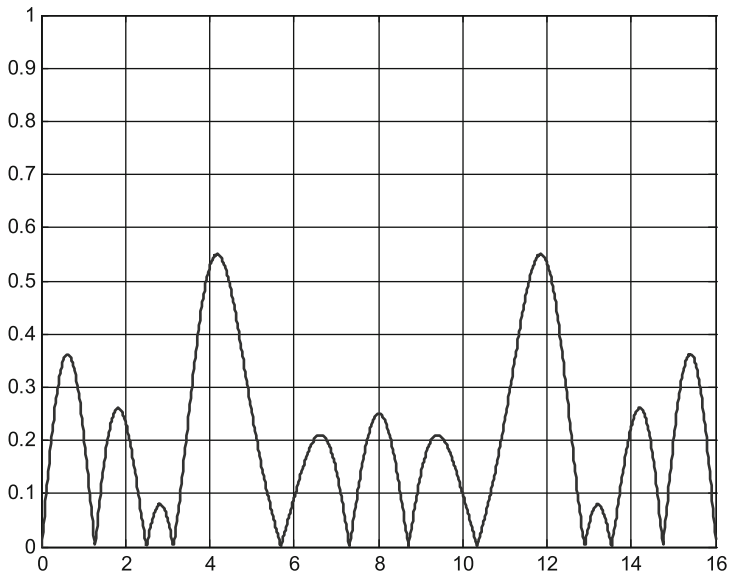


(b) A random symbol sequence.

**FIGURE 6.15**

Time-domain waveforms of a 16-subcarrier BPSK-OFDM transceiver system.

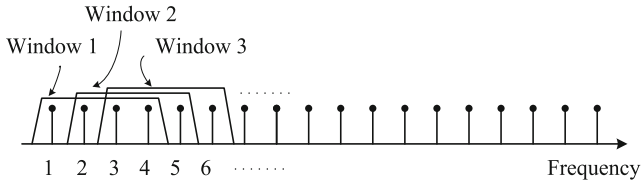


**FIGURE 6.16**

Subcarrier power window.

subcarriers have equal power [82]. Without power adjustment, $\pi_k$ is assumed to be equal for all subcarriers. In case of total power-constrained power adjustment, it is possible that all the power could be concentrated on a single subcarrier.

In window power-constrained power adjustment, if the power level of a certain subcarrier is lowered, the excess power can be transferred to the active subcarriers within a certain predefined sliding window. The total power for every grouping of $M$ subcarriers needs to be below the regulatory requirement, say $\pi_{\max}$. Then, the subcarrier power constraints are [218]

$$\sum_{k=l}^{l+M-1} \pi_k \leq \pi_{\max}, \quad \text{for all } l \tag{6.13}$$

and

$$\sum_{k=0}^{N-1} \pi_k \leq \pi_{\text{total}}. \tag{6.14}$$

For example, consecutive windows of subcarriers are shown in Figure 6.16. If the power level of a subcarrier in Window 1 is lowered, the power can be transferred to the other active subcarriers only within Window 1. When the power level of a subcarrier (say Subcarrier 3) is adjusted, the subcarrier power level must satisfy the window power constraints for all the member sliding windows (Window 1, Window 2, Window 3). A subcarrier power adjustment algorithm is shown in Figure 6.17 [220].

1. Initialize $\pi(0:N-1) = Z \sim f(x)$
2. Generate $L$ different power adjustment factors, $\{\pi_j\}_{j=0}^{L-1}$, or interleave $\pi$ using $L$ random interleavers (or other interleavers)
3. Check the FCC power constraint for each (interleaved) subcarrier power window $\pi_j$, using the sliding window algorithm presented in Figure 6.18
4. Modified symbols, $X_{\text{mod}} = X \cdot \sqrt{\pi_j}$
5. Choose $\pi_j$, which yields lowest PAPR

**FIGURE 6.17**

A subcarrier power adjustment based PAPR reduction algorithm.

```
1.  for k = 0 to (N − M + 1)
2.    for L = K to (K + m − 1)
3.      if π(l) < π_min
4.        π(l) = π_min
5.      end if
6.    end for
7.    S = Σ_{l=k}^{k+M−1} π(l)
8.    if S > π_max
9.      π(k : k+M−1) = π(k : k+M−1) * π_max/S
10.   end if
11. end for
12. return π
```

**FIGURE 6.18**

Sliding window power constraint.

A practical transmit power constraint is usually enforced as shown in Figure 6.18 to limit the total power across a frequency window of a specified width. For instance, the FCC has imposed requirements based on the amount of transmit power across a specified bandwidth in the UNII band [219]. These requirements are imposed, since these bands are usually unlicensed and the users are uncooperative.

### *Statistical Properties of PAPR*

Being a variant of OFDM, NC-OFDM also suffers from a high PAPR problem. When the number of deactivated subcarriers is large compared to the number of active subcarriers, the common assumption of the input symbols being identically and independently distributed does not hold. This results in different statistical properties for the PAPR of NC-OFDM signals relative to that for OFDM signals. The conventional OFDM systems inherently assume a contiguous set of subcarriers, whereas in a NC-OFDM system, the active subcarriers are colocated with the occupied subcarriers. Therefore, the PAPR reduction techniques proposed for the OFDM systems may need to be modified to avoid interfering with existing user transmissions. Moreover, the design requirements for PAPR reduction techniques are different from that of conventional OFDM systems. In this section, we present statistical analysis of PAPR for NC-OFDM signals and elaborate the design requirements of the PAPR reduction techniques for the NC-OFDM signals.

#### PAPR Distribution of an NC-OFDM Signal

Assume that the total number of subcarriers, $N$, is large. Then, applying the central limit theorem (CLT), $s(n)$ can be modeled as a zero-mean Gaussian distributed random variable with variance $\sigma^2 = N_u\sigma_D^2/N$, where $N_u$ is the number of active subcarriers and $\sigma_D^2$ is the variance of the input sequence [221]. Assuming the symbols are independent and identically distributed by CLT, the real and imaginary

parts of the $N$-point IFFT output have mutually independent Gaussian probability distribution function, $\mathcal{N}(0, \sigma^2)$. The instantaneous power of baseband signal, $s(n)$, is given by

$$\lambda = \Re\{s(n)\}^2 + \Im\{s(n)\}^2. \tag{6.15}$$

Therefore, the instantaneous power can be characterized as $\chi^2$ distribution with two degrees of freedom [72]:

$$f(\lambda) = \frac{1}{\sigma^2} \exp\left(-\frac{\lambda}{\sigma^2}\right), \quad \lambda \geq 0. \tag{6.16}$$

So, the cumulative distribution function (CDF) is given by [72]

$$\begin{aligned} Pr[\lambda < \lambda_0] &= \int_0^{\lambda_0} f(\lambda) d\lambda \\ &= 1 - e^{-\frac{\lambda_0}{\sigma^2}}. \end{aligned} \tag{6.17}$$

If $E\{|x(n)|^2\}$ is normalized to unity, then the CCDF of the PAPR is given by

$$Pr[\lambda > \lambda_0] = 1 - \left(1 - e^{-\frac{\lambda_0}{\sigma^2}}\right)^N. \tag{6.18}$$

However, this expression is not close to experimental results because the assumption made in deriving CCDF that the samples should be mutually uncorrelated is not true anymore when oversampling is used [222].

Several attempts have been made to more accurately determine the distribution of the PAPR for OFDM signals. In [222], it was claimed that the approximated CCDF for large $N$ is given by

$$Pr[\lambda > \lambda_0] \approx 1 - \left(1 - e^{-\frac{\lambda_0}{\sigma^2}}\right)^{\alpha N}, \tag{6.19}$$

where $\alpha = 2.8$. This approximation is fairly close to the experimental results when the number of active subcarriers is large; that is, $N \geq 64$.

### Maximum PAPR of an NC-OFDM Signal

It is known that the PAPR of an MPSK OFDM signal is always less than or equal to $N$, where $N$ is the total number of subcarriers. Note that, in OFDM, all of $N$ subcarriers are active. Now, consider the NC-OFDM signal with $p$ active subcarriers, where the input data symbols are chosen from an MPSK constellation such that $|A_k| = 1$.

The peak power of the NC-OFDM signal is given by [213]

$$\begin{aligned}\max_{0\le t\le T}|s(t)|^2 &= \max_{0\le t\le T}\left|\frac{1}{\sqrt{N}}\sum_{k=0}^{N-1}A_k e^{j2\pi kt/T}\right|^2\\ &\le \left(\frac{1}{\sqrt{N}}\sum_{k=0}^{N-1}\max|A_k|\right)^2\\ &\le \frac{p^2}{N}.\end{aligned} \tag{6.20}$$

Using the Parseval's relationship the average power of the NC-OFDM signal is given by [72]

$$\begin{aligned}E\{|s(t)|^2\} &= E\left\{\left|\frac{1}{\sqrt{N}}\sum_{k=0}^{N-1}A_k e^{j2\pi kt/T}\right|^2\right\}\\ &= \frac{1}{N}\sum_{k=0}^{N-1}\left\{E|A_k|^2\right\}\\ &= \frac{p}{N}.\end{aligned} \tag{6.21}$$

Then, the PAPR of the NC-OFDM signal is given from Equation (6.11) as follows:

$$\begin{aligned}\mathrm{PAPR}(s(t)) &= \frac{\max_{0\le t\le T}|s(t)|^2}{E\left\{|s(t)|^2\right\}}\\ &\le \frac{p^2/N}{p/N}\\ &\le p.\end{aligned} \tag{6.22}$$

Therefore, the maximum value of PAPR for the MPSK-modulated NC-OFDM signal with $p$ active subcarriers is equal to $p$, regardless of the total number of subcarriers, $N$.

### Design Requirements of PAPR Reduction Techniques for an NC-OFDM Signal

The conventional PAPR reduction techniques for OFDM systems inherently assume a contiguous set of subcarriers. Therefore, PAPR reduction techniques proposed for OFDM systems need to be adapted to a system employing NC-OFDM. In spectrum opportunistic systems, the active subcarriers are colocated with the occupied subcarriers. As a result, both intersymbol interference and intercarrier interference may cause distortion in the primary user transmissions. Therefore, time-domain-based or distortion-based techniques, such as clipping and filtering [223], and frequency-domain-based techniques assuming contiguous subcarriers, such as coding [207], cannot be used for reducing the PAPR of NC-OFDM signals. However,

frequency-domain PAPR reduction techniques are better suited, since it is easier to sort out the nulled subcarriers, avoiding any interference to existing user transmissions. The techniques, such as interleaving [224], SLM [210], and partial transmit sequences [211], need to be aware of the locations of the active subcarriers. Moreover, in a dynamic spectrum access network, the total number of active subcarriers and their locations might change continuously and the PAPR reduction techniques should be able to adapt to these changes.

## 6.5 CHAPTER SUMMARY AND FURTHER READINGS

In this chapter, we analyze several critical issues associated with OFDM-based cognitive radios and briefly discuss several proposed solutions. There are several significant ideas to draw from this chapter. First, spectral agility aimed at improving the utilization efficiency puts forth additional design constraints to conform to the spectral masks imposed by the regulatory agencies, to minimize the computations involved, and to avoid signal distortion during amplification due to the high PAPR nature of the multicarrier signals. In most cases, even though solutions have been proposed for the traditional contiguous subcarrier case, novel approaches need to be formulated for the noncontiguous subcarrier case.

Given that spectral agility is an important requirement for cognitive radio-oriented transceivers, it has to be noted that DFT-based OFDM is not the only modulation technique that achieves it. Several other techniques have been proposed by researchers over the past decade or so and compared with the classic DFT-based OFDM in terms of performance over widely differing channel conditions, as well as in terms of the involved implementation complexity of the transceiver. In [225], the authors introduce and show that $M$-band filter banks with overlapping basis functions can be used to design transmultiplexers with superior frequency-domain properties to those achievable with DFT filter banks. Consequently, the authors also show that the wavelet-transform-based discrete wavelet multitone has the DFT as a special case. A comparison of the BER performance in the presence of narrowband interference is reported in [226]. Other results on the waveform development using DWMT are reported in [227]. In [228, 229], equalization schemes for DWMT are proposed. While [228] presents simulated BER results to show that postdetection combining provides better performance, [229] presents linear and decision-feedback fractionally spaced receiver designs using modified filter banks. Reference [230] provides an overview of different orthogonal synthesis/analysis transform configurations. In [231], a comparison of the DFT-OFDM scheme with cosine-modulated filter banks (CMFBs) in terms of the prereceiver processing and performance in nonlinear phase channels is performed. Another paper that provides a comparison of different filter bank multicarrier techniques from the context of cognitive radio is [232]. In [233], a novel blind equalization algorithm for CMFB-based multicarrier transceivers is proposed and its BER performance is compared with the conventional OFDM system.

## 6.6 PROBLEMS

1 Using MATLAB, simulate the results shown in Figure 6.8, which is the impact of the raised cosine window with different roll-off factors on the side lobe power levels. Then, experiment with several other standard window functions and understand the roll-off nature of those windows.

2 Using MATLAB, simulate the efficiency of guard subcarriers shown in Figure 6.9 for the noncontiguous case. That is, assume several alternating sets of subcarriers occupied by licensed and unlicensed users and study the impact of the spectral spillage from the unlicensed bands to licensed portions of the spectrum. Vary the number of subcarriers in each noncontiguous set occupied by secondary users and observe the results.

3 Implement the standard Cooley-Tukey algorithm for the case of alternating licensed and unlicensed bands. Assign zeros to subcarriers used by licensed users. Store the number of additions and multiplications performed. Vary the number of zeros—that is, the number of licensed users in a given band of interest—and understand how the Cooley-Tukey algorithm is ineffective in reducing the number of computations as the unlicensed subcarriers reduce.

4 Figure 6.15 shows a plot of two discrete cases of the impact of PAPR for a BPSK-OFDM transceiver. Using Equation (6.11), plot the dependency of PAPR on the modulation scheme for a fixed number of subcarriers. Next, fix the modulation scheme and plot the PAPR as a function of the number of subcarriers.